PCCP

Accepted Manuscript

ROYAL SOCIETY OF CHEMISTRY

www.rsc.org/pccp

Electrocatalytic activity of Pt subnano/nanoclusters stabilized by pristine graphene nanosheets

Yi Shen*[a], Zhihui Zhang[a], Kaijun Xiao[a] and Jingyu Xi*[b]

[a] College of Light Industry and Food Sciences, South China University of Technology, Guangzhou, 510640, China. Email: feyshen@scut.edu.cn;

[b] Lab of Advanced Power Sources, Graduate School at Shenzhen, Tsinghua University, Shenzhen 518055, China. Email: xijingyu@gmail.com.

Abstract Downsizing the Pt particle to atomic level in the electro-catalysts is highly desirable to enhance its utilization efficiency in fuel cells. In this study, Pt subnano/nanoclusters were stabilized by the pristine graphene nanosheets (GNS) derived from chemical vapor deposition and the resulting Pt/GNS hybrids were examined as catalysts for electro-oxidation of alcohols (methanol, ethanol, ethylene glycol and glycerol). In spite of the strong hydrophobic surface, the GNS was proved to be a promising catalyst support because the edges and defects in the GNS could effectively anchor and stabilize the Pt subnano/nanoclusters. The Pt/GNS catalyst showed an extremely high electrochemical active surface area and superior catalytic activity for alcohol oxidation compared with the commercial Pt/carbon black catalyst. The enhanced catalytic performance was attributed to the presence of the discrete Pt subnano/nanoclusters as well as the modulation of the electronic properties of Pt nanoparticles through the chemical interaction of Pt atoms with the edges and defects of the GNS support.

Introduction

Direct alcohol fuel cells (DAFCs) as promising alternative power sources for portable electronics and vehicles have attracted great attention because of the high power density, low operating temperature, and easy storage and transport of liquid fuels. However, the high cost and limited supply of the noble metal Pt in the catalyst remain the critical obstacle inhibiting the wide commercialization of DAFCs.[1] To address this problem, considerable effects have been directed in developing novel catalysts with enhanced catalytic activity as well as platinum utilization efficiency.[2-8] Downsizing the Pt particles, in particular, the miniaturization to atomic level could significantly enhance the specific active area and the catalytic performance of Pt in fuel cells.[9-11] However, the mass production and stabilization of Pt subnanoclusters are very challenging due to the high surface energy. Recently, graphene nanosheets (GNS) have been extensively studied as catalyst support.[12-17] It has been demonstrated that GNS can effectively stabilize the ultrafine Pt nanoparticles (NPs) and that the GNS-supported catalysts show enhanced activity for alcohol oxidation. Nevertheless, there is no unanimous conclusion on the origin of the support effects of GNS. For instance, Yoo *et al.*[18] synthesized the Pt subnanoclusters stabilized by GNS and

observed the significant support effects of the GNS on the catalytic activity. It was suggested that the high activity of the Pt/GNS catalyst was arisen from the modifications on the electronic structures of Pt subnanoclusters due to the chemical interaction between the Pt clusters and graphene,[19-21] via the ligand effects.[22] Different from this viewpoint, it was also proposed that the superior catalytic activity of the Pt/GNS catalysts was attributed to the presence of oxygen-containing groups in the surface of GNS, which were favorable for the removal of the poisoning intermediates,[23-25] based on the so-called bifunctional mechanism.[26] In most cases, bifunctional and ligand effects are coexistent in electrocatalysis. It is difficult to disentangle these two factors on the enhancement of catalyst performance.[27-30]

In the literature, the GNS catalyst supports were most commonly prepared from the reduction of exfoliated graphite oxide and inevitably contained abundant functional groups such as hydroxyl, epoxides, carbonyl and carboxyl.[31] These oxygen-containing groups played an important role on anchoring and stabilizing Pt NPs. However, the presence of these groups also significantly reduced the conductivity and stability of the GNS support. In contrast to the reduced graphene oxide, the GNS derived from chemical vapor deposition (CVD) contain less oxygen-containing groups and possess higher conductivity.[31] Up to now, the CVD process is extensively used to produce GNS. However, limited studies on using this type of GNS as catalyst support are reported.[32] It is a fact that the surface of the GNS derived from the CVD process under higher temperatures are extremely hydrophobic, which is considered to be detrimental to the dispersion of Pt NPs.[33] In our previous work,[34] we reported a facile and economical method for the mass production of GNS by chemical vapor deposition. Herein, we endeavored to use the resulting GNS as catalyst support for the synthesis of Pt/GNS catalysts. In spite of the fact that the GNS are free of oxygen-containing groups, the edges and defects of the GNS could serve as active sites to stabilize the ultrafine Pt NPs. The synthesis and assembly of the Pt subnanoclusters on the GNS support were achieved by the facile polyol-assisted reduction method. It was found that the Pt/GNS hybrid showed superior catalytic activity for the oxidation of alcohols (methanol, ethanol, ethylene glycol (EG) and glycerol).

Experimental section

Synthesis and purification of GNS support

The GNS support were prepared by CVD and further purified by acid etching and sedimentation separation, as described in our previous work.[34] The GNS support consisted of few-layered graphene sheets with 10 layers or less per sheet. The surface area of the GNS was 247 $m^2 \cdot g^{-1}$ as determined by the Brunauer-Emmett-Teller (BET) method. It is noted that many edges and defects are present in the GNS support (see Figure S1 in the Electronic Supplementary Information (ESI)).

Synthesis of Pt/GNS catalyst

The Pt/GNS catalyst was synthesized using the polyol reduction method.[35,36] The details of the experimental procedures are as follows: 100 mg of GNS support was dispersed into 150 ml of ethylene glycol by alternative ultrasonication and magnetic stirring to form a stable suspension. 1.2 g of NaOH was added into the mixture. After the complete dissolution of NaOH, 450 μL of H_2PtCl_6 solution (8 wt. %, Sigma Aldrich) was also added into the mixture. Subsequently, the mixture was transferred into an oil bath and the reduction was carried out at 180 ºC for 15 min under continuous magnetic stirring. After cooling to room temperature, the mixture was separated by centrifuge and thoroughly washed with ethanol. The resulting catalyst was dried at 80 ºC overnight using a vacuum oven. The nominal weigh percentage of Pt in the resulting Pt/GNS catalyst was ca. 15%. The actual Pt weight percentage in the Pt/GNS catalyst was measured to be 12.4% by inductively coupled plasma analysis atomic emission spectrometer (ICP-AES).

Characterization of catalyst

A transmission electron microscope (JEM2010, JEOL) were used to observe the morphology of the samples. High-resolution TEM micrographs were obtained from an alternative JEM-2010F (JEOL) microscope. The samples for the TEM tests were prepared by ultrasonication of the powdered samples in ethanol and evaporation of one drop of the suspension onto a carbon film supported on a mesh copper grid. An energy dispersive X-ray (EDX) analyzer equipped in the TEM and an axis-ultra X-ray photoelectron spectrometer (Kratos-Axis Ultra System) with monochromatized Al-Kα radiation were used to analyze the elemental composition of the samples. Raman spectra were recorded with a Renishaw Raman microscope using 633-nm excitation at room temperature. The actual Pt content in the Pt/GNS catalyst was analyzed by ICP analysis. About 1 mg of catalyst sample was dissolved in 10 mL of aqua regia at room temperature overnight. 1-2 mL of the suspension was taken using a pipette and carefully injected into a nanofiltration needle to remove undissolved residues. The resulting solution was diluted with deionized water and then submitted for analysis using an ICP-AES (Varian PE/Sciex ELAN 6100DRC).

Electrochemical measurements were carried out using a three-electrode cell connected to a PARSTAT 2273 electrochemical station (AMETEK, Inc. USA.). A gold patch (effective area 1×1 cm) coated with a thin layer of catalyst ink was used as working electrode. The cover density of the catalyst on the gold patch was ca. 200 μg/cm^2. A saturated calomel electrode (SCE) and Pt gauze were used as reference and counter electrodes, respectively. Cyclic voltammograms were recorded in the potential range -0.2 to 1.0 V at a scan rate of 50 mV s^{-1} while linear

sweeping voltammetry (LSV) curves were recorded at a scan rate of 1 mV s^{-1}. A solution of 1M alcohol and 1M H_2SO_4 was used as electrolyte. The electrochemical active surface area (ECSA) of the catalyst was determined from the hydrogen absorption-desorption process in 1 M H_2SO4 solution. The chronoamperometric curves were obtained under an applied potential of 0.6 V. Before the test, the solution was saturated with N_2 gas for 20 min. Several activation scans were performed until reproducible voltammograms were obtained. Only the last voltammograms were used for comparing the catalytic activity of the specified catalysts. The measurements were conducted at 25 ºC and all potentials in this report were referenced to the SCE.

Results and Discussion

The morphological structure, the particle size and the dispersion of Pt NPs were examined by transmission electron microscopy (TEM). Figure 1 shows the TEM micrographs of the ultrafine Pt NPs decorated on the GNS support. It can be seen that the Pt NPs are preferentially anchored to the graphene edges as shown in Figures 1A. It is noteworthy that Pt clusters are well dispersed on the GNS support without formation of large aggregates. One thousand Pt NPs were randomly selected to determine the size distribution and the histogram of Pt NPs in the Pt/GNS catalyst is shown in Figure S2-A (see the ESI). The Pt NPs possessed diameters ranging from 0.8 to 2.2 nm. A representative high-resolution TEM micrograph (see Figure S3 in the ESI) shows the lattice fringes with a spacing of 2.3 Å that corresponds to the Pt (111) plane in face-centered cubic Pt crystals. A careful inspection on the TEM micrographs revealed that some Pt NPs could also be found on the surface of the GNS as shown in Figure 1C. The corresponding histogram of Pt NPs was shown in Figure S2-B. It was indicated that the Pt NPs located on the surface of the GNS had an average diameter of 1.1 nm and that many sub-nanometer Pt NPs could be observed. It is also noted that the number of Pt NPs located on the surface of GNS support is less than that of Pt NPs attached onto the edges of GNS. This could be explained from the structural characteristics of the GNS support. Numerous graphene edges were present in the GNS support as shown in Figure S1. The elemental composition of the Pt/GNS was examined by EDX as shown in Figure 1D. The presence of Cu peak in the EDX spectrum was attributed to the TEM grid. Based on the TEM results, it was demonstrated that the graphene edges and surface defects in the GNS support were the active sites for the nucleation and stabilization of Pt NPs.[37, 38] The interaction of Pt NPs with the dangling bonds in the graphene edges and carbon vacancies effectively stabilized the Pt NPs, which resulted in the formation of the discrete Pt subnano/nanoclusters attached on the edges and defects of the GNS support.

XPS was employed to analyze the electronic properties of Pt in the catalyst. Figure 2 shows the high-resolution deconvoluted Pt 4f XPS spectra (The O 1s and C 1s spectra are shown in Figure S4). The spectra were corrected using the C 1s signal located at 284.5 eV. The Pt 4f

spectrum consisted of the doublets of Pt 4f7/2 and 4f5/2. The deconvolution of the Pt 4f5/2 peak yielded two peaks at 75.9 and 75.0 eV while the deconvolution of the Pt 4f7/2 peak yielded two peaks at 72.6 and 71.7 eV, which could be assigned to $Pt^{2+}$and Pt^{0} oxidation states, respectively.[39] The presence of Pt^{2+} could probably due to the surface oxidation during the experimental processes. The Pt NPs in the Pt/GNS catalyst exhibited higher binding energy as compared with that of the single Pt crystal, *i.e.*, 71.1 eV, indicating that the Pt in the Pt/GNS catalyst exhibited a "cationic" behavior.[40] This was attributed to the presence of the large number of Pt atoms with low coordination numbers such as edge and corner Pt atoms in the Pt subnanoclusters, which resulted in the strong π-d hybridization between the Pt filled d orbitals and carbon p* empty orbitals. Such hybridization could shift the d-band center of Pt NPs away from the Fermi level as reported by Cini *et al*.[35] and subsequently lead to decreases in adsorption energy of CO molecules on Pt surface based on the d-band center criterion.[41, 42] Therefore, the interface interactions between the Pt NPs and GNS support could significantly enhance the electro-catalytic activity of the Pt NPs.[43, 44]

The significant support effects of the GNS were further studied using Raman spectroscopy. The Raman spectra of the pristine GNS support and the Pt/GNS are shown in Figure 3. For comparison, the spectra were normalized to give approximately the same relative intensity. Typical peaks were clearly visible at ca. 1330 (D-mode), 1575 (G-mode), and 2670 cm^{-1} (2D-mode). For the pristine GNS, the intensity ratio of I_D/I_G was about 0.63, confirming the existence of numerous edges and defects in the GNS. For the Pt/GNS catalyst, the I_D/I_G was slightly increased to 0.65, indicating that the structure of graphene was well-preserved after the assembly of Pt NPs. The intensity ratio of I_{2D}/I_G was closely related to the Fermi energy (E_F) of the graphene as reported by Casiraghi *et al*.[45] The relationship between the intensity ratio of I_G/I_{2D} and the Fermi level position of graphene could be expressed as

$$\sqrt{I_G/I_{2D}} = C'\left(\gamma_{ep} + 0.07\left|E_F\right|\right)$$

where C' is a constant and γ_{ep} is the energy of emission phonons.[45] The Pt/GNS catalyst exhibited an I_G/I_{2D} ratio of 1.5, which was larger than that of the pristine GNS (0.8) (see Figure S5 in the ESI). Based on the equation, it could be inferred that, upon the assembly of Pt clusters on the GNS support, the Fermi level of GNS was lowered. This was also attributed to the interface interaction of Pt NPs with the GNS support as indicated by the XPS results.[21]

The electrochemical catalytic activity of the Pt/GNS catalyst was characterized. A commercial Pt/carbon black (denoted as Pt/C) was used as reference for comparison. Figure 4 shows the cyclic voltammograms (CVs) of the Pt/GNS and Pt/C catalyst in a solution 1M H_2SO_4. The electrochemical active surface area (ECSA) of the catalyst was determined based on the

hydrogen adsorption charge in the scan range of -0.2 – 0 V. The ECSA value of the Pt/GNS catalyst was 112 m^2/g, which was much higher than that of Pt/C catalyst (63 m^2/g). The high ECSA of the Pt/GNS catalyst was attributed to the smaller particle size of the discrete Pt NPs, which provided more accessible active sites in the Pt/GNS catalyst. It is worth noting that the Pt reduction peak in the Pt/GNS catalysts is located around 0.51 V while the Pt reduction peak in the Pt/C catalyst is located around 0.48 V as shown in the CVs. It is indicated that the oxide in the Pt/GNS catalyst is relatively easier to be reduced than that in the Pt/C catalyst. This could be related to the smaller particle size of Pt NPs in the Pt/GNS catalyst and the interaction of Pt with the GNS support.[46]

Figure 5 shows CV curves of alcohol electro-oxidation at the Pt/GNS and Pt/C catalysts. The current density shown in the CVs was normalized by the mass of the Pt loading. For the four alcohols, the Pt/GNS catalysts showed much higher catalytic activity compared with the Pt/C catalyst. The Pt/GNS catalyst exhibited peak current densities of 316, 449, 205 and 120 $mA \cdot mg^{-1}$ Pt for the oxidation of methanol, ethanol, EG and glycerol, respectively, which were 1.53, 1.93, 2.18 and 1.9 times those of the Pt/C catalyst. Considering the larger ECSA of the Pt/GNS than that of Pt/C catalyst (the former was 1.77 times of the latter), the current densities normalized by ECSA were comparable for the two catalysts. Therefore, it was demonstrated that the utilization efficiency of Pt in the Pt/GNS catalyst was much higher than that in the Pt/C catalyst, which was mainly attributed to the ultrafine size of Pt clusters in the Pt/GNS catalyst. To study the stability of the catalysts, the CV tests in 1 M methanol – 1 M H_2SO_4 with 50 cycles were carried out as shown Figure 6. It was shown that the Pt/GNS and Pt/C catalyst showed similar degradation rates on current density (8 – 9% degradation after 50 cycles). No distinct morphological changes were observed in the spent samples after 50 cycles (see Figure S7 in the ESI). Furthermore, linear sweeping voltammetry (LSV) curves showed that the onset potential for methanol oxidation at the Pt/GNS catalyst was about 380 mV, which was 50 mV more negative than the potential at the Pt/C catalyst (see Figure S5 in the ESI). The Pt/GNS catalyst exhibited a maximum current density of 63 $mA \cdot mg^{-1}$ Pt at 0.6 V while the Pt/C catalyst had a maximum current density of 39 $mA \cdot mg^{-1}$ Pt at 0.61 V for the oxidation of methanol as shown in the LSV curves, which were consistent with the CV results. The durability of the catalysts was further evaluated by amperometric measurements. Figure 7 shows chronoamperometric curves for alcohol oxidation at a constant potential of 0.6 V. The current densities showed a rapid decay during the initial period because of the insufficiency of alcohol reactants. It can be seen that the current densities of the Pt/GNS catalyst are higher than those of Pt/C catalysts. The Pt/GNS catalyst has current densities of 167, 151, 32 and 39 $mA \cdot mg^{-1}$ Pt after 300 second for the oxidation of methanol, ethanol, EG and glycerol, respectively, which were 2.3, 6.6, 1.7 and 5.6

times those of the Pt/C catalyst. These results indicated that the Pt/GNS catalyst had better performance than the Pt/C catalyst.

It was confirmed that the Pt/GNS catalyst exhibited superior catalytic activity for alcohol oxidation. Since the GNS catalyst support in this study was synthesized by the catalytic deposition of methane at high temperatures (> 800 ºC), limited oxygen-containing groups but numerous edges and surface defects were present in the surface of the GNS support. It could be inferred that the enhanced catalytic activity of Pt/GNS catalyst was mainly arisen from the dispersion of the ultrafine Pt NPs as well as the modification on the Pt electronic structure due to the chemical interaction between the GNS support and Pt NPs. The uniform dispersions of Pt subnano/nanoclusters on the GNS support not only provided abundant accessible active sites for alcohol oxidation as confirmed by the ECSA of the Pt/GNS catalyst, but also the large number of Pt atoms with low coordination numbers in the Pt subnanoclusters which showed enhanced catalytic activity for alcohol oxidation. In addition, the interaction of Pt NPs with the graphene edges and surface defects greatly affected the electronic structure of the Pt NPs as indicated by the XPS results, which could probably be the main reason for the significant enhancement on the catalytic activity.

Conclusion

In summary, it is demonstrated from this study that the GNS synthesized by the CVD process can be used as an effective catalyst support. In spite of the strong hydrophobic surface of the GNS, the presence of the edges and defects on the GNS is favorable to anchor and stabilize the Pt NPs. The support effects of the GNS were also reflected from the modulation on the electronic properties of the Pt NPs through the chemical interaction of Pt with the edges and defects of the GNS support. The Pt/GNS catalyst exhibited superior catalytic activity for alcohol oxidation compared with the commercial Pt/C catalyst. It can be concluded that the superior catalytic activity of the Pt/GNS catalyst is attributed to the uniform dispersion of the ultrafine Pt NPs as well as the modification of the electronic structures of Pt particles. Our studies provide a new avenue for the exploration of advanced graphene-supported electro-catalysts with high Pt utilization efficiency and catalytic performance.

Acknowledgments

We are grateful for the financial support from “the Fundamental Research Funds for the Central Universities (ZB20140003)”

Additional information

Electronic supplementary information (ESI) on Figures S1-S5 is available.

Notes and References

1. H. A. Gasteiger, S. S. Kocha, B. Sompalli and F. T. Wagner, *Appl. Catal. B: Environ.* 2005, **56**, 9-35.
2. T. Toda, H. Igarashi and M. Watanabe, *J. Electrochem. Soc.* 1998, **145**, 4185-4188.
3. F. Maillard, G. Q. Lu, A. Wieckowski and U. Stimming, *J. Phys. Chem. B* 2005, **109**, 16230-16243
4. I. E. L. Stephens, A. S. Bondarenko, U. Grønbjerg, J. Rossmeisl and I. Chorkendorff, *Energy Environ. Sci.* 2012, **5**, 6744-6762.
5. X. L. Wang, C. Li and G. Q. Shi, *Phys. Chem. Chem. Phys.* 2014, **16**, 10142-10148
6. J. Suntivich, Z. C. Xu, C. E. Carlton. J. Kim, B. H. Han, S. W. Lee, N. Bonnet, N. Marzari, L. F. Allard, H. A. Gasteiger, K. Hamad-Schifferli and S. H. Yang, *J. Am. Chem. Soc.* 2013, **135**, 7985-7991.
7. R. T. Mu, Q. Fu, H. Xu, H. Zhang, Y. Y. Huang, Z. Jiang, S. Zhang, D. L. Tan and X. H. Bao, *J. Am. Chem. Soc.* 2011, **133**, 1978-1986.
8. J. F. Chang, L. G. Feng, C. P. Liu, W. Xing and X. L. Hu, *Energy Environ. Sci.* 2014, **7**, 1628-1632
9. K. Sasaki, H. Naohara, M. Y. Choi, Y. Cai, W. F. Chen, P. Liu and R. R. Adzic, *Nat. Comm.* 2012, **3**, 1115.
10. K. Yamamoto, T. Imaoka, W. J. Chun, O. Enoki, H. Katoh, M. Takenaga and A. Sonoi, *Nat. Chem.* 2009, **1**, 397-402.
11. A. U. Nilekar, S. Kotaro, C. A. Farberow, R. R. Adzic and M. Mavrikakis, *J. Am. Chem. Soc.* 2011, **133**, 18574-18576.
12. C. G. Hu, H. H. Cheng, Y. Zhao, Y. Hu, Y. Liu, L. M. Dai and L. T. *Adv. Mater.* 2012, **24**, 5493-5498.
13. H. P. Cong, X. C. Ren and S. H. Yu, *ChemCatChem* 2012, **4**, 1555-1559
14. S. J. Guo, S. J. Dong and E. K. Wang, *ACS NANO*. 2010, **4**, 547-555.
15. J. Zhao, H. Yu, Z. S. Liu, M. Ji, L. Q. Zhang and G. W. Sun, *J. Phys. Chem. C* 2014, **118**, 1182-1190.
16. H. J. Huang, H. Chen. D. P. Sun and X. Wang, *J. Power Sources* 2012, **204**, 46-52.
17. F. H. Li, Y. Q. Guo, Y. Liu, J. Yan, W. Wang and J. P. Gao, *Carbon* 2014, **67**, 617-626
18. E. Yoo, T. Okata, T. Akita, M. Kohyama, J. Nakamura and I. Honma, *Nano Lett.* 2009, **9**, 2255-2259
19. R. Siburian, T. Kondo and J. Nakamura, *J. Phys. Chem. C* 2013, **117**, 3635-3645.
20. E. Cho, E. N. Yitamben, E. V. Iski, N. P. Guisinger and T. F. Kuech, *J. Phys. Chem. C* 2012, **116**, 26066-26071.
21. Y. T. Kim, M. A. Matin and Y. U. Kwon, *Carbon* 2014, **66**, 691-698.
22. P. Liu, A. Logadottir and J. K. Nørskov, *Electrochim. Acta* 2003, **48**, 3731-3742.
23. S. Sharma, A. Ganguly, P. Papakonstantinou, X. P. Miao, M. X. Li, J. L. Hutchison, M. Delichatsios and S. Ukleja, *J. Phys. Chem. C* 2010, **114**, 19459-19466.
24. Y. J. Hu, P. Wu, Y. J. Yin, H. Zhang and C. X. Cai, *Appl. Catal. B: Environ.* 2012, **111**, 208-217.
25. Y. Z. Li, Y. Yu, J. G. Wang, J. Song, Q. Li, M. D. Dong and C. J. Liu, *Appl. Catal. B: Environ.* 2012, **125**, 189-196.
26. J. Rossmeisl, P. Ferrin, G. A. Tritsaris, A. U. Nilekar, S. Koh, S. E. Bae, S. R. Brankovic, P. Strasser and M. Mavrikakis, *Energy Environ. Sci.* 2012, **5**, 8335-8342.

27. C. Roth, N. Benker, T. Buhrmester, M. Mazurek, M. Loster, H. Fuess, D. C. Koningsberger and D. E. Ramaker, J. Electrochem. *J. Am. Chem. Soc.* 2005, **127**, 14607-14615.
28. P. Waszczuk, G. Q. Lu, A. Wieckowski, C. Lu, C. Rice and R. I. Masel, *Electrochim. Acta* 2002, **47**, 3637-3652.
29. F. Vigier, C. Coutanceau, F. Hahn, E. M. Belgsir and C. Lamy, *J. Electroanal. Chem*. 2004, **563**, 81-89.
30. Y. Ishikawa, M. S. Liao and C. R. Cabrera, *Surf. Sci.* 2000, **463**, 66-80
31. M. M. Liu, R. Z. Zhang and W. Chen, *Chem. Rev.* 2014, DOI: 10.1021/cr400523y
32. C. S. Shan, H. Tang, T. L. Wong, L. F. He and S. T. Lee, *Adv. Mater.* 2012, **24**, 2491-2495.
33. H. J. Huang and X. Wang, *J. Mater. Chem. A* 2014, **2**, 6266-6291
34. Y. Shen and A. C. Lua, *Sci. Rep.* 2013, **3**, 3037.
35. W. Li, C. Liang, W. Zhou, J. Qiu, Z. Zhou, G. Sun, Q. Xin, *J. Phys. Chem. B* 2003, **107**, 6292-6299.
36. O. Winjobi, Z. Zhang, C. Liang , W. Li, *Electrochim. Acta* 2010, **55**, 4217-4221.
37. Y. A. Kim, T. Hayashi, J. H. Kim and M. Endo, *J. Energy Chem.* 2013, **22**, 183-194.
38. I. Kvande, J. Zhu, T. J. Zhao, N. Hammer, M. Ronning, S. Raaen, J. C. Walmsley and D. Chen, *J. Phys. Chem. C* 2010, **114**, 1752-1762.
39. C. Nethravathi, E. A. Anumol, M. Rajamathi and N. Ravishankar, *Nanoscale*. 2010, **3**, 569-571.
40. M. Cini, M. Decrescenzi, F. Patella, N. Motta, M. Sastry, F. Rochet, R. Pasquali, A. Balzarotti and C. Verdizzi, *Phys. Rev. B* 1990, **41**, 5685-5695.
41. B. Hammer and J. K. Nørskov, *Surf. Sci.* 1995, **343**, 211-220.
42. Y. Y. Tong, C. Rice, A. Wieckowski and E. Oldfield, *J. Am. Chem. Soc.* 2000, **122**, 1123-1129
43. J. Nakamura and T. Kondo, *Top Catal.* 2013, **56**, 1560-1568.
44. S. M. Zhang and S. L. Chen, *J. Power Sources* 2013, 240, 60-65.
45. C. Casiraghi, *Phys. Rev. B* 2009, **80**, 233407.
46. P. Panagiotopoulou, A. Christodoulakis, D. I. Kondarides and S. Boghosian, *J. Catal.* 2006, **240**, 114-125

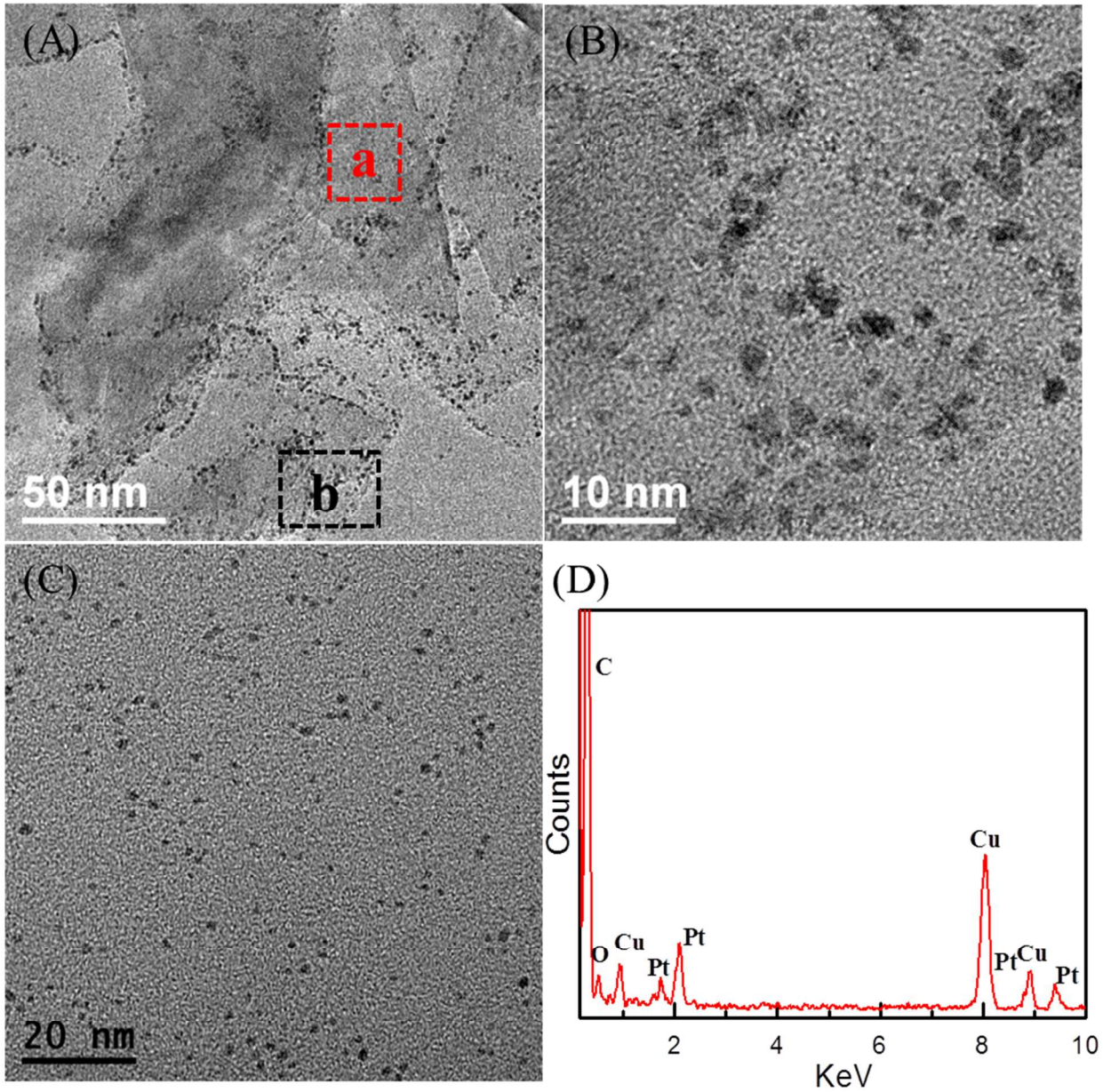

Figure 1 TEM and EDX analysis of the Pt/GNS catalyst. (A) Overview of the Pt/GNS catalyst, (B) magnification of the region marked "a" in (A), (C) magnification of the region marked "b" in (A) and (D) elemental composition of the Pt/GNS catalyst.

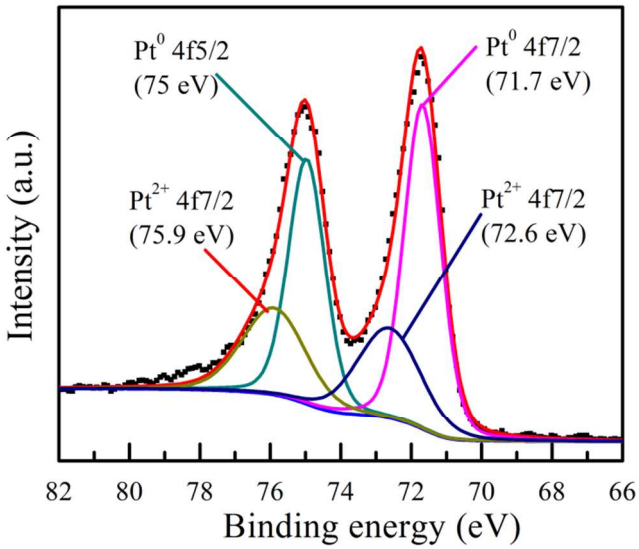

Figure 2 High-resolution XPS spectra of the Pt 4f in the Pt/GNS catalyst.

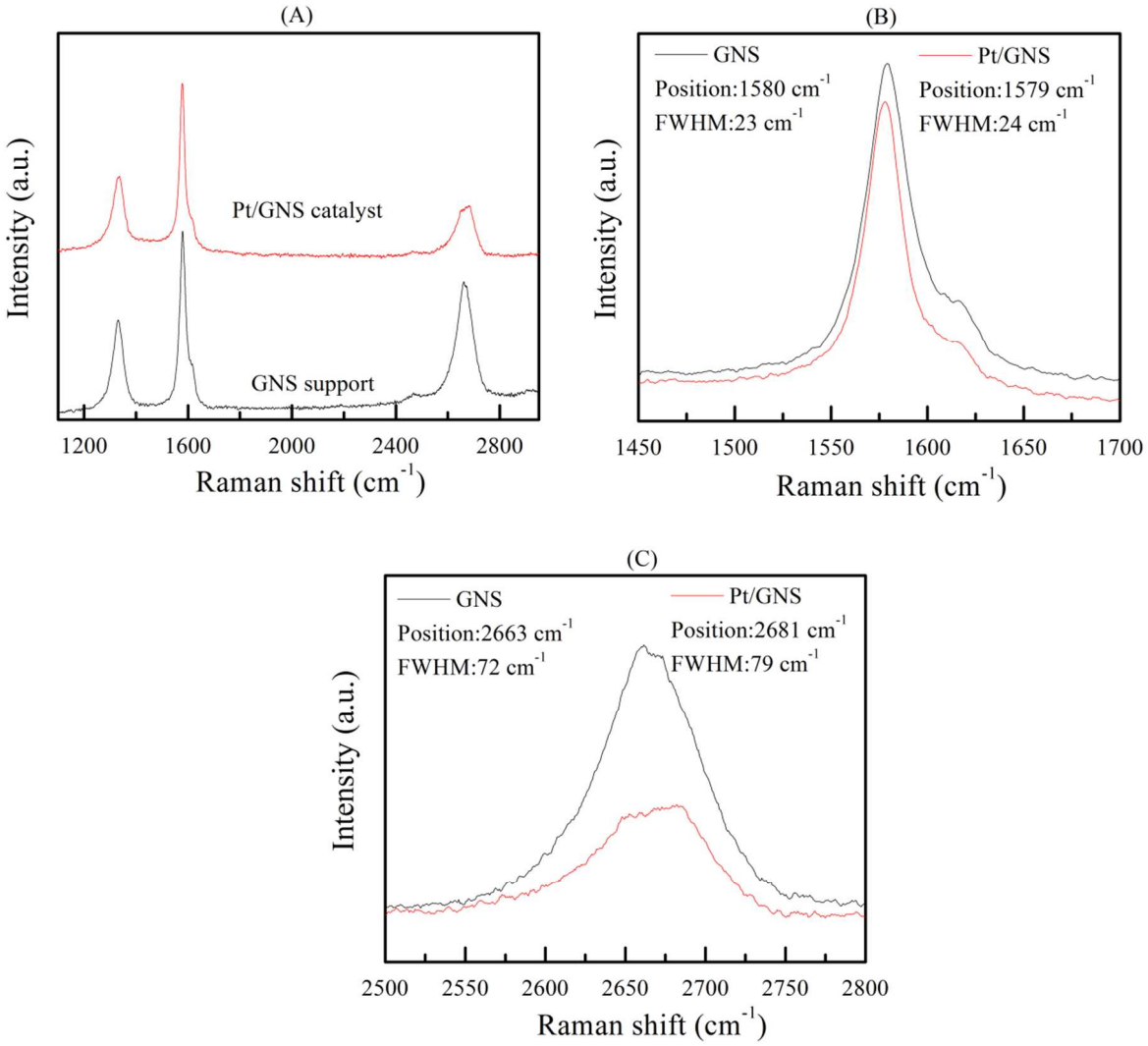

Figure 3 Raman spectra of the pristine GNS and Pt/GNS catalyst (A) Overall spectra, (B) D band peak, and (C) 2D band peak.

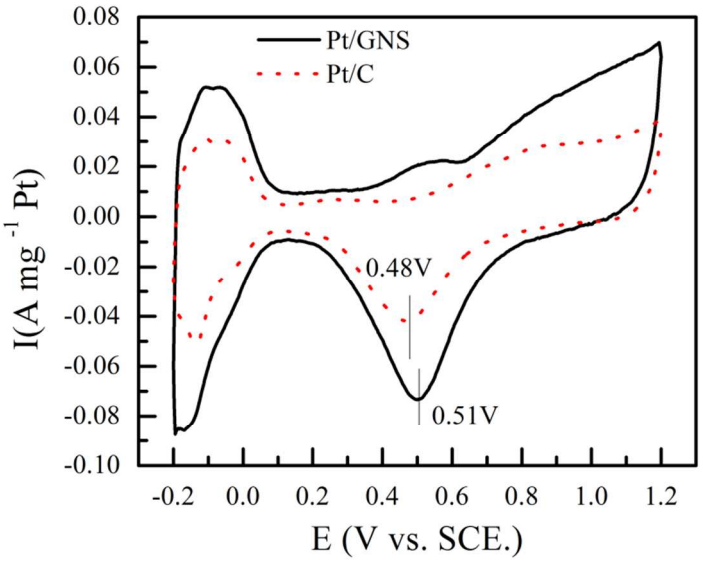

Figure 4 Cyclic voltammetry curves of Pt/C (dotted line) and Pt/GNS catalyst (solid line) at 25 ºC in 1 M H_2SO_4 with a scan rate of 50 mV s^{-1}.

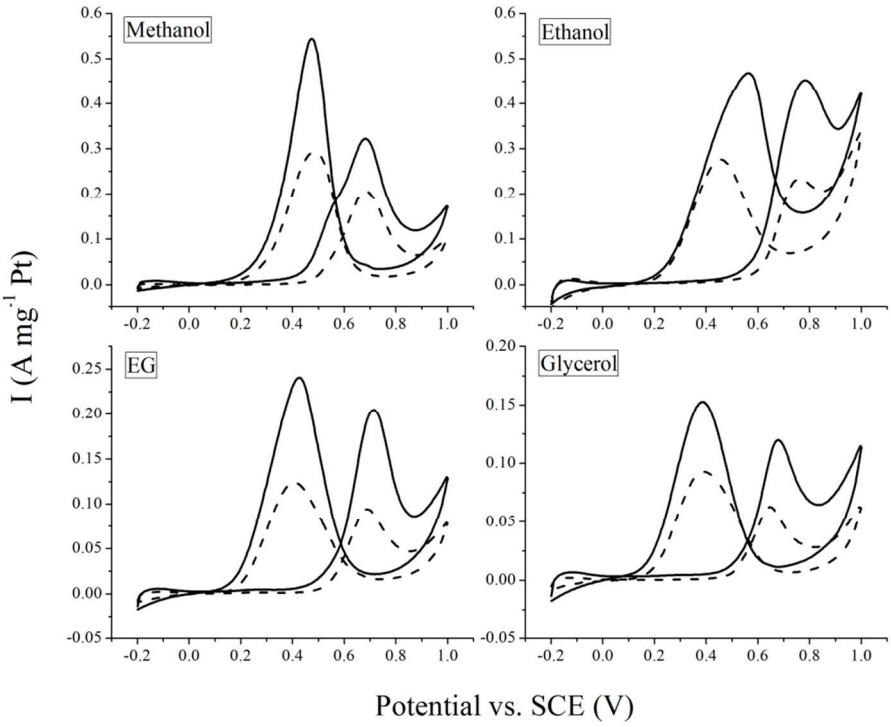

Figure 5 Cyclic voltammetry curves of alcohol electro-oxidation at the Pt/C (dotted line) and Pt/GNS catalyst (solid line) at 25 ºC in 1 M alcohol – 1 M H_2SO_4 in the potential range of 0.2 to 1.0 V vs. SCE with a scan rate of 50 mV s^{-1}.

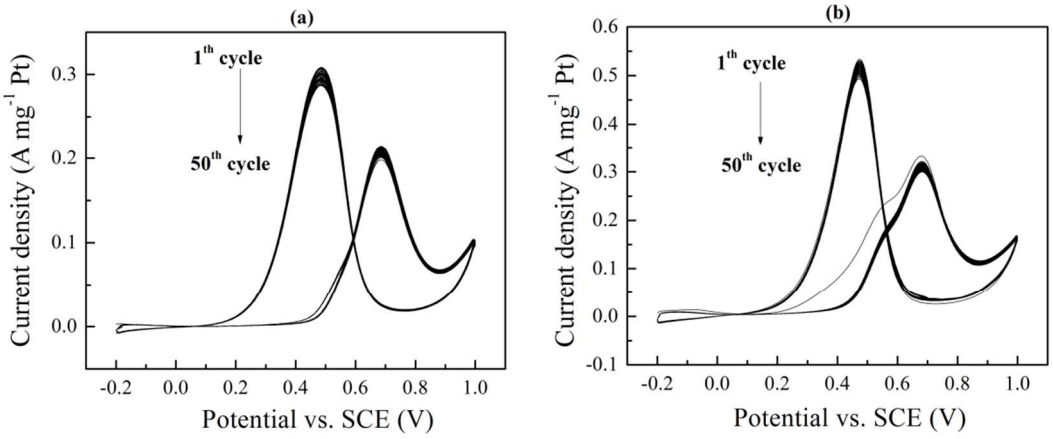

Figure 6 Stability of the catalysts (a) Pt/C and (b) Pt/GNS catalyst studied by cyclic voltammetry at 25 ºC in 1 M methanol – 1 M H_2SO_4 in the potential range of 0.2 to 1.0 V vs. SCE with a scan rate of 50 mV s^{-1}.

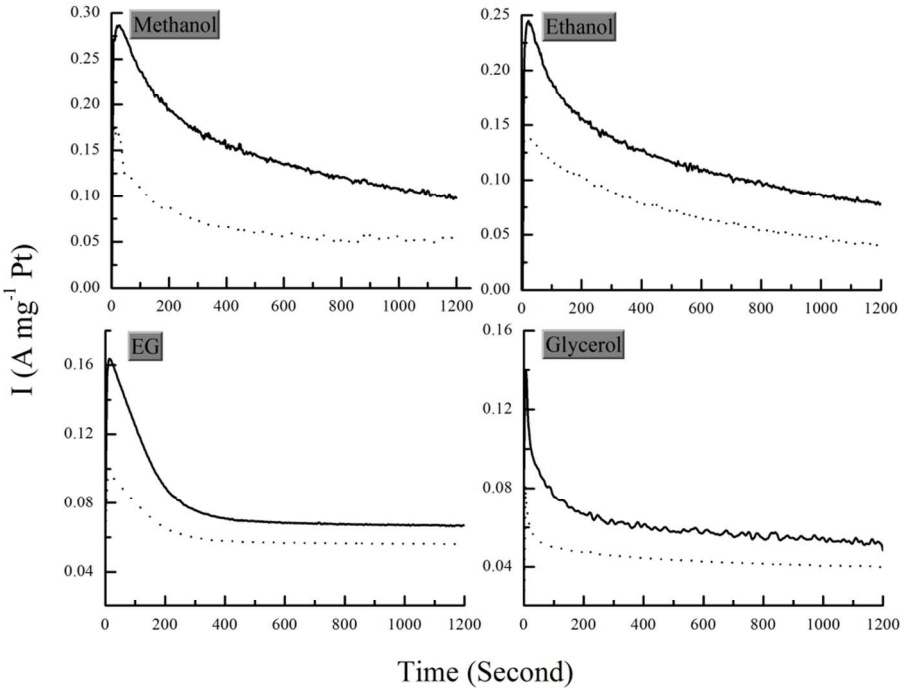

Figure 7 Chronoamperometric curves of Pt/C (dotted line) and Pt/GNS (solid line) recorded 25 ºC in 1 M alcohol – 1 M H_2SO_4 at a constant potential of 0.6 V.